Two distinct phases of North Atlantic eastern subpolar gyre and warming hole evolution under global warming

Two Distinct Phases of North Atlantic Eastern Subpolar Gyre and Warming Hole Evolution under Global Warming

ROHIT GHOSH,[a,b] DIAN PUTRASAHAN,[a] ELISA MANZINI,[a] KATJA LOHMANN,[a] PAUL KEIL,[a] RALF HAND,[c,d] JÜRGEN BADER,[a,e] DANIELA MATEI,[a] AND JOHANN H. JUNGCLAUS[a]

[a] *Max Planck Institute for Meteorology, Hamburg, Germany*
[b] *Department of Meteorology, University of Reading, Reading, United Kingdom*
[c] *Institute of Geography, University of Bern, Bern, Switzerland*
[d] *Oeschger Centre for Climate Change Research, University of Bern, Bern, Switzerland*
[e] *Uni Climate, Uni Research, and Bjerknes Centre for Climate Research, Bergen, Norway*

(Manuscript received 1 April 2022, in final form 7 November 2022, accepted 14 November 2022)

ABSTRACT: The North Atlantic subpolar gyre (SPG) plays a crucial role in determining the regional ocean surface temperature (SST), which has profound implications on the surrounding continental and coastal climate. Here, we analyze the Max Planck Institute-Grand Ensemble global warming experiments and show that the SPG can evolve in two distinct phases under continuous global warming. In the first phase, as the global mean surface temperature approaches 2-K warming, the eastern SPG intensifies in combination with a weakening Atlantic meridional overturning circulation (AMOC), accompanied by a cooling of subpolar North Atlantic SST, known as the warming hole. The associated oceanic fingerprint matches with the observations over the last 15 years, where an intensification and cooling of the eastern SPG is related to salinity reduction at the eastern side of the SPG. However, for further warming beyond 2 K, in spite of a continuous decline in the AMOC, a northward shift of the mean zonal wind extends the subtropical gyre northward with an associated disruption of the eastern SPG intensification, resulting in the cessation of the warming hole. Therefore, a shift from the initially dominating oceanic drivers to the atmospheric driver results into a two-phase evolution of the North Atlantic Ocean SPG circulation and the associated SST under continuous global warming.

KEYWORDS: North Atlantic Ocean; Atmosphere-ocean interaction; Nonlinear dynamics; Ocean dynamics; Gyres; Climate change

1. Introduction

The North Atlantic gyres play a vital role in transporting heat, salt, and nutrients throughout the ocean basin (Hátún et al. 2005; Palter et al. 2005), influencing the biological distribution and the ecological system (Carpenter and Smith 1972; Colton et al. 1974; Law et al. 2010; Jenkins 1982; Hátún et al. 2009, 2016, 2017). Especially the distribution of heat by the subpolar gyre (SPG) has been shown to have a prominent effect on the downstream climate over Europe (Hermanson et al. 2014; Moreno-Chamarro et al. 2017b,a; Ghosh et al. 2017; Moffa-Sánchez and Hall 2017; Jalali et al. 2019). However, the effect of anthropogenic warming on SPG are hardly explored (Oldenburg et al. 2018; Menary and Wood 2018) and still remains highly uncertain (Reintges et al. 2017). Previous studies using satellite observations of sea surface height (SSH), available from 1993 onward, have suggested a complex nature of SPG evolution. The SPG went through a decline during the 1990s (Häkkinen and Rhines 2004; Hátún et al. 2005), which has been attributed to atmospheric internal variability, such as the North Atlantic Oscillation (Böning et al. 2006; Lohmann et al. 2009b,a). Further studies with a longer observational record show a slowdown in the decline from 2005 onward (Daniault et al. 2011; Robson et al. 2016; Chafik et al. 2019). However, the observational period is still very limited, making it difficult to decipher if such recent evolution can be attributed to natural variability or to forced response from global warming. Moreover, other observational studies suggest different characteristics of evolution between the western and eastern parts of the SPG (Foukal and Lozier 2017; Hátún and Chafik 2018). The observations show a continuous increase of SSH (Hátún and Chafik 2018), which is mainly attributed to the thermodynamic effect of sea level rise (Foukal and Lozier 2017). In the case of dynamical changes, the western SPG has not changed significantly, whereas the eastern and central parts show clear decadal-scale variations in a reverse association with Atlantic meridional overturning circulation (AMOC) (Zhang 2008). These decadal-scale variations show a strengthening eastern SPG trend in the last decade (Chafik et al. 2019), in association with a weakening trend in AMOC. Likewise, given that, under global warming, the AMOC is suggested to weaken (Manabe and Stouffer 1993; Stocker and Schmittner 1997; Schmittner et al. 2005; Cheng et al. 2013; Rahmstorf et al. 2015), the

Denotes content that is immediately available upon publication as open access.

Supplemental information related to this paper is available at the Journals Online website: https://doi.org/10.1175/JCLI-D-22-0222.s1.

Corresponding author: Rohit Ghosh, r.ghosh@reading.ac.uk

DOI: 10.1175/JCLI-D-22-0222.1

question remains if such an associated observed strengthening eastern SPG is predominantly driven by natural variability or bears a forced response to increasing greenhouse gas concentrations.

Because the observational records are limited, we address the aforementioned open question using the Max Planck Institute-Grand Ensemble (MPI-GE) (Maher et al. 2019), which captures the observed eastern SPG variability (shown in section 3) and would allow us to separate the forced response from internal variability (Li and Ilyina 2018). We mainly use the experiment of 1% CO_2 increase per year (mentioned hereafter as 1% CO_2), which facilitates an investigation of the ocean dynamical response of the North Atlantic gyres under transient forcing. First, we show that under increasing CO_2 the forced changes in SPG could occur in two distinct phases and further more we find that the North Atlantic warming hole only intensifies in the first phase due to the increase in anomalous meridional heat transport divergence from a strengthening eastern SPG.

2. Data and methods

The MPI-GE simulations are performed with the Earth system model MPI-ESM1.1 in its low-resolution configuration (Giorgetta et al. 2013). The MPI-ESM1.1 consists of the ocean model MPIOM with GR1.5 grid configuration (Marsland et al. 2003; Jungclaus et al. 2013). The GR1.5 grid has two poles among which one is over southern Greenland, which allows a high resolution of 15 km around the main regions of North Atlantic water mass transformation (Jungclaus et al. 2008). The MPIOM also consists of 40 unevenly spaced depth levels. The atmospheric component of MPI-ESM is ECHAM6.3 with horizontal resolution of roughly 1.8° and 47 vertical levels (Stevens et al. 2013). Further, MPI-ESM1.1 has an ocean biogeochemistry component HAMOCC5.2 (Ilyina et al. 2013) and a land component JSBACH-3.00 (Reick et al. 2013).

We use the MPI-GE 1% CO_2 increase per year, historical (1850–2005) and RCP8.5 scenario (2006–99) experiments with 100 ensemble members each, which enables us to distinguish the mean response from the internal variability (Maher et al. 2019). The transient experiment of 1% CO_2 increase per year uses the same initial conditions as in the historical experiments and is performed for 150 years. We use this experiment to understand the changes in the North Atlantic gyre circulation for two phases, representing two consecutive global warming periods of 2 K. In the first phase, the annual global mean near surface temperature (GMST) increases from 0- to 2-K anomaly with respect to the preindustrial level and in the second phase from 2 to 4 K. In doing so, each phase represents an equal amount of global warming and the comparison of the oceanic parameters for the two phases informs on deviations from a linear response to global warming (Manzini et al. 2018).

Following a recent study on atmospheric circulation changes using the same data (Manzini et al. 2018), the initial climate state (denoted 0 K) is defined by the ensemble mean of the first 10 years (years 1–10). The climate states at 2- and 4-K GMST warming are, respectively, defined by 10-yr ensemble means around the year when the GMST reached 2 K (years 77–86) and 4 K (years 133–142) with respect to the initial climate state (note that these timings are slightly different from those reported in (Manzini et al. 2018), because of their smoothing applied prior to the timing identification). Due to a large ensemble size, a 10-yr mean is suitable to capture the climate mean state especially under strong CO_2 forcing in a transient simulation. The forced dynamic response in the first phase is defined as the difference of the climate state at 2 K minus the state at 0-K GMST warming. Similarly, the second phase response represents the difference of the climate state at 4 K minus that at 2-K GMST warming.

The temporal evolution of the latitudinally averaged barotropic streamfunction (BSF) is constructed as a Hovmöller diagram to illustrate the transient changes in SPG circulation and SST with time. This is performed by subtracting the ensemble mean of the BSF for the first year of the simulation from that of the next years.

For the difference of the ensemble means, a statistical significance test has been applied for the difference of the mean using the Student's t distribution considering a sample size of 100. Only the regions significant below a p value of 0.05 are shown in the color shading without stippling.

The observed sea surface height is a gridded product at 0.25° resolution of the monthly mean absolute dynamic topography from the SSALTO/DUACS DT2014 multisatellite altimeter data (Pujol et al. 2016) for the period 1993–2019 taken from the http://marine.copernicus.eu/services-portfolio/access-to-products/. The salinity and ocean temperature observations are from the Grid Point Value of the Monthly Objective Analysis using the Argo data (MOAA-GPV) (Hosoda et al. 2008) provided by JAMSTEC for the period 2001–19. The observed trends are calculated through performing linear regression with time as the independent variable. For the statistical significance of the trend, Student's t test is being performed where the p values are determined using incomplete beta function on the t statistic.

The basinwide meridional heat transport (MHT) is calculated using the variables ocean meridional velocity (V) and the potential temperature (θ). The V and θ are integrated in depths (dz) and in longitudes (dx) following a certain latitude (y) over the North Atlantic Ocean to obtain the MHT [$Q(y, t)$] at that latitude. We chose the depth space integration due to it being the most common way of representing MHT as well as the AMOC (Yeager 2015). According to Bryan (1982), the MHT can be expressed as

$$Q(y,t) = \int\int \rho C_p V \theta \, dx \, dz, \tag{1}$$

where ρ is the ocean water potential density and C_p is the specific heat capacity of the ocean water at constant pressure. This could also be expressed as in Griffies et al. (2016):

$$Q(y,t) = \int\int \rho C_p (\overline{V} + V')(\overline{\theta} + \theta') \, dx \, dz, \tag{2}$$

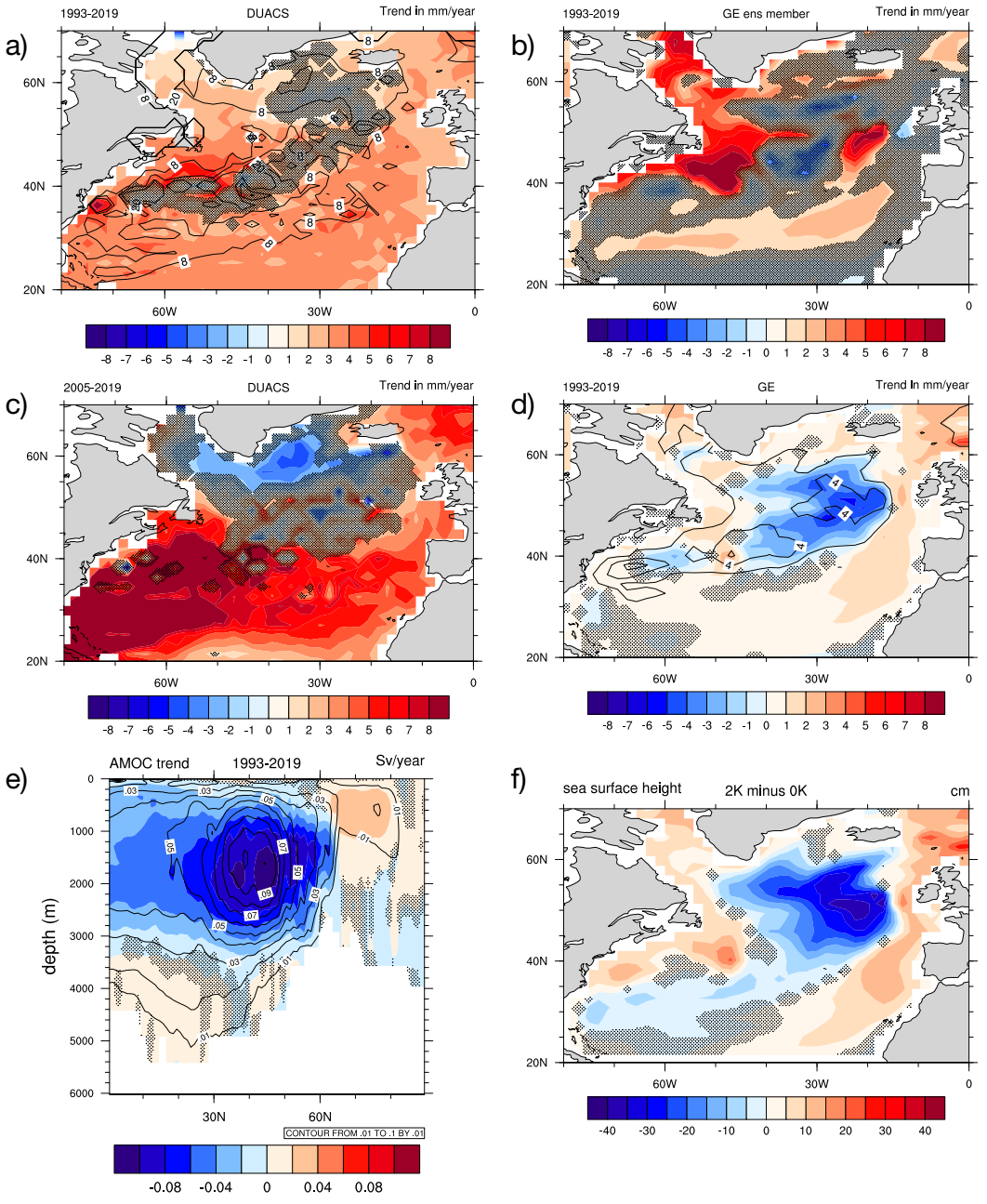

FIG. 1. (a) The annual mean sea surface height (SSH) trend (shading) from the SSALTO/DUACS satellite altimeter data (Pujol et al. 2016) for the period 1993 to 2019. Contours show the standard deviation of the 10-yr running mean SSH at each grid indicating the regions of observed decadal-scale variations. (b) The same annual SSH trend for the period 1993–2019 in one of the ensemble members of the MPI-GE historical+RCP8.5 scenario experiments, showing a similar trend pattern of SSH as in observations (mm yr^{-1}). (c) As in (a), but the SSH trend for the period 2005–19 (mm yr^{-1}), under a weakening phase of lower-latitude AMOC condition. The ensemble mean (shading) and ensemble standard deviation (contours) of trend of the annual mean (d) SSH and (e) AMOC (Sv yr^{-1}) in MPI-GE from historical+RCP8.5 experiments for the entire observed period of 1993–2019. (f) The difference of the ensemble mean SSH (m) between 2-K global mean surface air temperature (GMST) warming and 0-K GMST warming levels in the MPI-GE 1% CO_2 experiment. For all figures, unstippled regions are significant at $p < 0.05$, and negative values of the SSH over the subpolar region denote anomalous cyclonic circulation or the strengthening of the subpolar gyre, whereas positive values denote anomalous anticyclonic circulation or weakening.

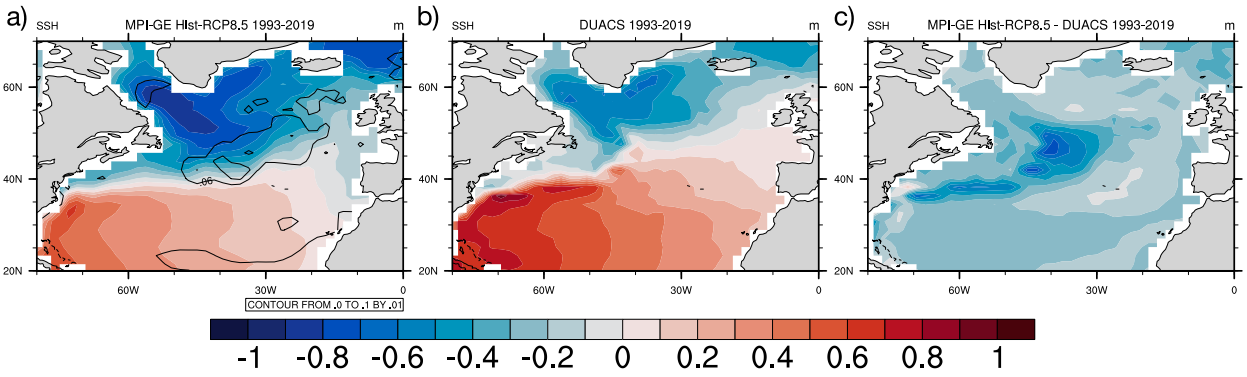

FIG. 2. (a) The ensemble mean of the annual mean sea surface height (SSH; m) over the period 1993–2019 (colors), representing climatology of gyres over the North Atlantic Ocean in the MPI-GE historical+RCP8.5 scenario experiments, and contours represents the ensemble standard deviation. (b) The observed climatology of gyres, as an average annual mean SSH (m) from SSALTO/DUACS for the same period of 1993–2019. (c) The difference in climatology of gyres in MPI-GE from (a) and in observations from (b).

where $\overline{V}$, $\overline{\theta}$ are the zonal means and V', θ' are the respective deviations from the zonal means. Hence, the MOC and gyre components of the MHT are the following:

$$Q(y,t)_{\mathrm{MOC}} = \int\int \rho C_p \, \overline{V}\,\overline{\theta}\, dxdz, \tag{3}$$

$$Q(y,t)_{\mathrm{gyre}} = \int\int \rho C_p \, V'\theta'\, dxdz. \tag{4}$$

The other two components of the MHT are negligible compared to the MOC and gyre components.

3. Strengthening eastern SPG under weakening AMOC: Observations and MPI-GE

In the DUACS multisatellite altimetry observations of sea surface height (SSH) for the entire period of 1993–2019, there is no significant trend over the eastern SPG region (shadings in Fig. 1a). It is due to prominent decadal scale variations over the eastern side of the SPG (contours in Fig. 1a), which has been identified in previous literature (Hátún and Chafik 2018; Chafik et al. 2019). We find a similar nature in some of the individual realizations of the MPI-GE for the same time period from historical simulations continuing to RCP8.5 scenarios, indicating the capability of the model to simulate the observed characteristic (Fig. 1b). We find the highest variance of strength in the trend over the eastern SPG region in MPI-GE, further affirming that the model captures the highly variable nature of the observed eastern SPG (black contours in Fig. 1d). This also shows the need of a large ensemble simulation to detect the forced response over the eastern part of the SPG.

The ensemble mean trend, which depicts the anthropogenically forced component of the response, shows a significant strengthening over the eastern side of the model climatological SPG (Fig. 1d). This strengthening eastern SPG occurs in association with a weakening AMOC (Fig. 1e). Interestingly, such association in observations in decadal time scale variations has been previously suggested (Zhang 2008), we indeed observed such eastern SPG strengthening and AMOC weakening after 2005 (Fig. 1c). Hence, the model forced response and its subsurface signature (shown in Fig. 4) shows dynamically consistent AMOC–eastern SPG response that has been identified in observations on decadal time scales. Moreover, the results from the CMIP5 multimodel ensemble trend also showed a strengthening of the eastern part of the climatological SPG over the observed period [Fig. 7b in Richter et al. (2017)].

By contrast, the SSH in the western part shows an increasing trend (Fig. 1a), which possibly only represents the thermodynamic effect of sea level rise (Foukal and Lozier 2017).

The observed strengthening over the recent decades is more northwestward than in the MPI-GE, which could be related to their respective extensions of climatological eastern side of the SPG (Figs. 2a,b). The differing eastward extension is due to a more zonal and hence further eastward reaching nature of the North Atlantic Current (NAC) in the model (Jungclaus et al. 2013) (Fig. 2c). Further, in general the climatological SPG circulation seems to be slightly stronger in the model compared to observations (Fig. 2c).

In line with the results from the Historical and RCP8.5 scenario runs, a strengthened eastern to central SPG arises also during the first 2-K global warming in the MPI-GE 1% CO_2 experiment (Fig. 1f), confirming that this trend is likely caused by greenhouse gas forcing. Does the strengthening continue with further warming under increasing CO_2? And what could be the possible underlying physical mechanisms? Above all, how does it relate to the North Atlantic subpolar SST? We use the standard ocean model variable, barotropic streamfunction (BSF), as a conventional and direct estimate to explore these questions using the MPI-GE 1% CO_2 experiment.

4. Two distinct phases of North Atlantic gyre evolution

Under the CO_2 forced global warming, the evolution of the North Atlantic gyres in MPI-GE has two distinct phases. During the first 2 K of global warming, in accordance with the SSH fields, the BSF shows an intensification of the eastern to central SPG (Fig. 3a). A strengthening eastern SPG is also found in observations on multidecadal time scales and linked to the weakening phase of the AMOC (Zhang 2008). However, for a

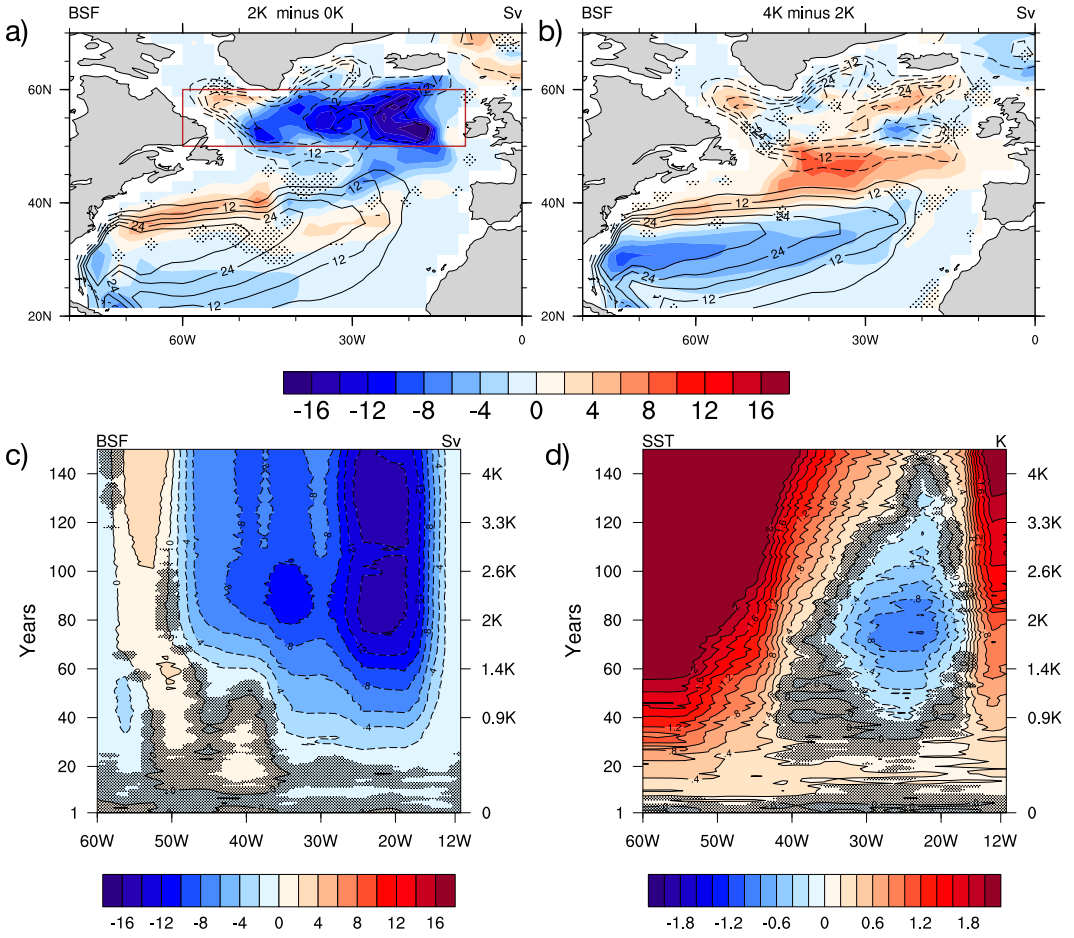

FIG. 3. The difference of the ensemble mean annual barotropic streamfunction (BSF; colors; Sv) (a) between 2-K global mean surface air temperature (GMST) warming and 0-K GMST warming levels and (b) between 4-K GMST warming and 2-K GMST warming levels in the MPI-GE 1% CO_2 increase per year experiment. Contours are the ensemble mean annual BSF or the climatology for the 0- and 2-K GMST warming state in (a) and (b), respectively. Negative values of BSF denote cyclonic circulation and positive values denote anticyclonic circulation. (c) For the same experiment, the Hovmöller diagram of the difference of the ensemble mean annual BSF on a certain year from year 1, averaged over the latitude band 50°–60°N and encompassing the longitude range covered by 60°–10°W [brown box in (a)]. Negative values indicate intensification/strengthening of the subpolar gyre, whereas positive values indicate weakening. (d) As in (c), but for the sea surface temperature (SST; K) averaged over the latitude band 45°–55°N (black box in Fig. 4e). The right side of the *y* axis shows the GMST warming level to a corresponding year. Unstippled regions are statistically significant at $p < 0.05$.

GMST warming above 2 K until 4 K, the eastern to central SPG does not intensify further, but rather stabilizes (Fig. 3b). Further, the northern part of the subtropical gyre (STG) extends further north, inducing an anticyclonic circulation over the intergyre region. Therefore, these two phases of global warming show two distinct features in the forced changes over North Atlantic eastern SPG and intergyre regions.

The southern to central part of STG and western SPG show a continuous weakening in both phases of GMST warming. The STG weakening can be explained through wind driven circulation changes (Fig. S1 in the online supplemental material), which is a robust feature in CMIP5 models (Beadling et al. 2018). The weakening western SPG, especially over the Labrador Sea, is anticipated to be a consequence of a reduced Labrador Sea deep convection, which is also known as one of the main causes of the lower latitude AMOC weakening in the models under anthropogenic forcing (Hátún and Chafik 2018).

Over the SPG region (50°–60°N), the longitudinal cross section of the anomalous BSF reveals that the eastern to central SPG strengthening is initiated from the eastern side (Fig. 3c). This part of the forced changes in the anomalies is twice as large as its initial climatological strength in the model by the time of 2-K GMST warming. Progressing from the eastern to the western side of the SPG, the strengthening starts at a later stage of the GMST warming. The cause of the predominant eastern SPG strengthening to a weakening AMOC can be explained through the mechanism of increasing density gradient

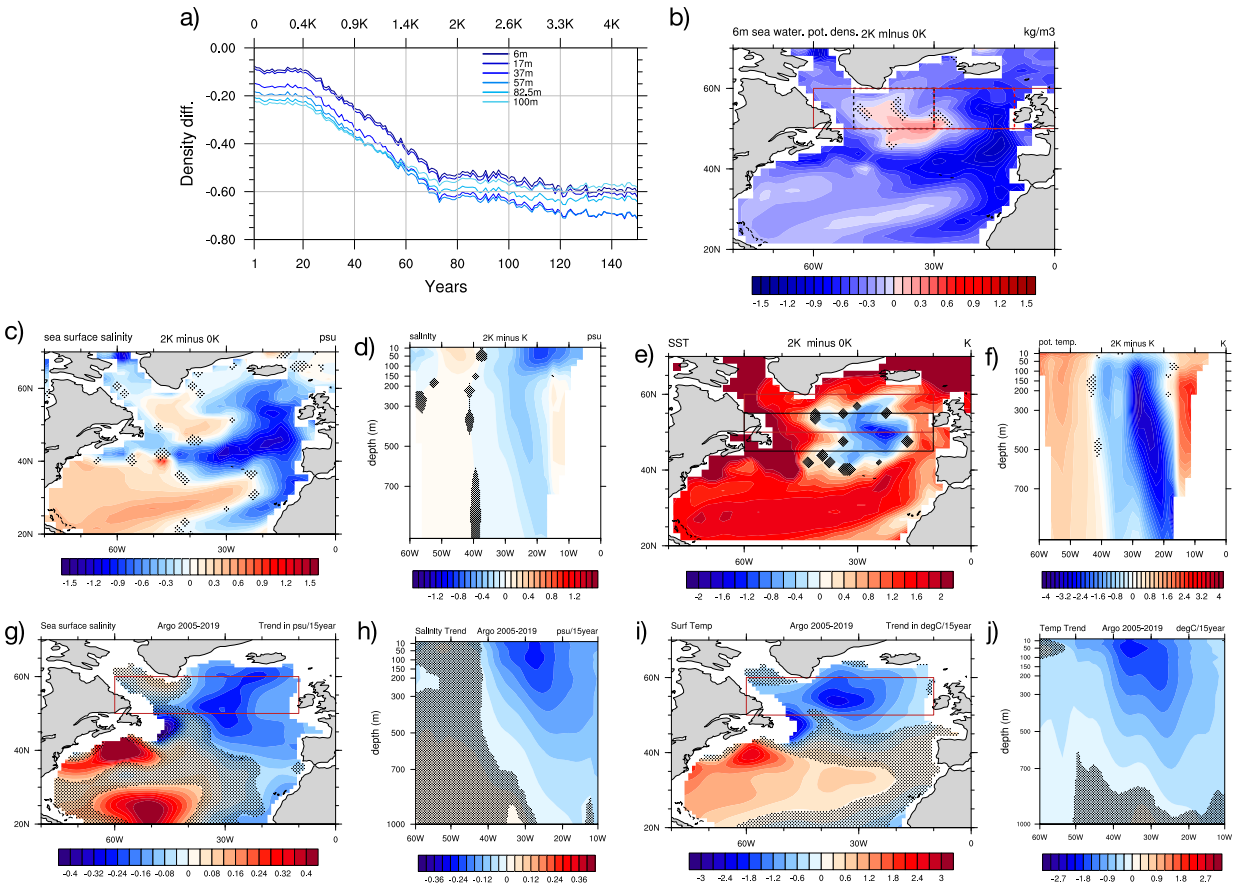

FIG. 4. (a) Temporal evolution of the ensemble mean annual potential density difference (kg m^{-3}) between the red and black dashed boxes in (b) for depths until 100 m. (b) The difference of the ensemble mean annual 6-m potential density between 2-K global mean surface temperature (GMST) warming and 0-K GMST warming levels in the MPI-GE 1% CO_2 increase per year experiment. (c),(e) As in (b), but for sea surface salinity (psu) and sea surface temperature (K), respectively. The difference of the same 2- and 0-K warming state in a longitude–depth profile for (d) salinity and (f) ocean temperature until 1000-m depth averaged over the brown box in (b) (50°–60°N, 0°–60°W). (g) The annual mean 10-m salinity [considered as sea surface salinity; psu (15 yr)$^{-1}$] and (i) sea surface temperature trend [°C (15 yr)$^{-1}$] in the Argo float observations from MOAA-GPV (Hosoda et al. 2008) for the period consisting lower-latitude AMOC weakening as part of decadal variability from 2005 to 2019. (h),(j) Corresponding associated longitude–depth profile until 1000 m averaged over the brown box in (g) (50°–60°N, 10°–60°W). Unstippled regions are statistically significant at $p < 0.05$.

from the east to the center of the SPG (Zhang 2008; Levermann and Born 2007; Born and Stocker 2014), which we elaborate in the next section.

a. 0–2-K warming: Eastern SPG intensification association with increasing density difference from the east to center

A possible mechanism behind the SPG strengthening could be the increase of the negative density difference from the east to the center of the SPG after the first 20 years (0.4-K GMST warming) of the simulation (Fig. 4a), in line with the beginning of the SPG intensification at the eastern side (Fig. 3c). Increase in negative density difference indicates that the center of the gyre is becoming relatively denser, leading to a cyclonic rotation anomaly and hence increasing SPG strength (Levermann and Born 2007; Born and Stocker 2014). The increase in negative density difference is mainly due to the significant decrease of the upper ocean layer density at the east of the SPG in the first phase of the 2-K global warming (Fig. 4b). This decrease in the density can be found deep inside the ocean reaching more than 700 m (not shown).

The density reduction at the eastern side of the SPG is mainly associated with salinity reduction (Figs. 5a,b), which shows a similar pattern of decrease, especially over the eastern side of the SPG (Fig. 4c). Interestingly, in accordance with previous findings (Robson et al. 2016; Bryden et al. 2020), we can detect a similar significant decrease for the observed surface salinity trend from the Argo floats at the east of the observed SPG after 2005 (Fig. 4g). The trends of the observed salinities at depths also resemble the changes of the salinity for the first 2 K of warming in the MPI-GE experiment, albeit with a reduced magnitude (Figs. 4d,h). Moreover,

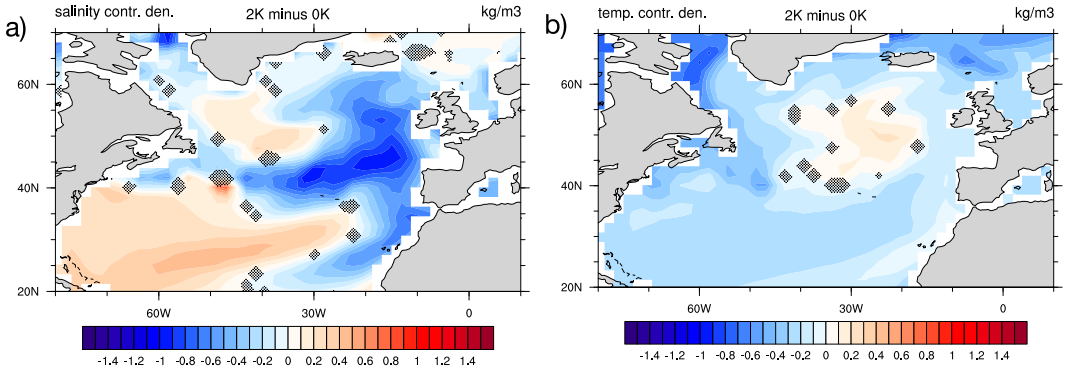

FIG. 5. (a) The difference of the ensemble mean annual sea surface salinity contribution to density (kg m^{-3}), between 2-K global mean surface air temperature (GMST) warming and 0-K GMST warming levels in the MPI-GE 1% CO2 increase per year experiment. (b) As in (a), but for the surface temperature contribution to density (kg m^{-3}). Unstippled regions are statistically significant at $p < 0.05$.

in accordance with the differences in observed and model locations of the eastern SPG strengthening (Fig. 1c), the observed salinity trend is located west of where we find it in the MPI-GE (Fig. 4d). This indicates a close association of the underlying dynamics with the NAC in both observations and in the MPI-GE. Due to the strong association with the NAC, the density reduction on the eastern side of the SPG could be the result of a weakening AMOC (Smeed et al. 2014, 2018; Robson et al. 2016; Hand et al. 2020) (Fig. S4c, red curve in Fig. 9), which can lead to reduced salt transport through the North Atlantic Current and can create a condition of less dense water at the eastern side of the SPG.

Apart from salinity, the associated temperature changes also partly contribute to increase the density at the SPG center and hence to increase the east-to-center density difference (Fig. 5b). This temperature contribution to SPG density changes stems from the SPG cooling in MPI-GE as a forced response, widely known as North Atlantic warming hole (Fig. 4e) (Drijfhout et al. 2012; Rahmstorf et al. 2015). The depth structure of this temperature response shows that the center of cooling stays west of the center of salinity response (cf. Figs. 4d,f). Hence the cooling induced density changes at the center adds to the salinity induced density changes at the east to increase the zonal density difference. A very similar feature is found in observations too after 2005, where the temperature structure shows a cooling over SPG with its center (30°–40°W) to the west of the center of the salinity changes (25°–30°W) (Figs. 4i,j).

The winds are suggested to have played a partial role in the recent observed strengthening of the SPG after 2005 (Robson et al. 2016; Chafik et al. 2019), though the long term changes are indicated to be associated with the buoyancy forcing (Robson et al. 2016). For the first 2 K of warming in the 1% CO_2 experiment, the wind-driven Sverdrup (1 Sv $\equiv 10^6$ m^3 s^{-1}) transport changes do not show an increase in cyclonic circulation over the eastern SPG and hence cannot explain the forced strengthening of the eastern SPG in the MPI-GE (Fig. S1). This indicates that the observed wind driven changes might be part of the internal variability, while the observed salinity driven changes could contain the anthropogenically forced response.

b. *2–4-K warming: Northward extension of STG by northward shift of the zonal wind and warming hole cessation*

The STG and SPG are separated by the NAC, which, if it moves northward, would cause a northward extension of the STG. An important factor in setting the strength and position of the NAC is the mean zonal wind above the extratropical North Atlantic. In the 2–4-K GMST warming phase, the 10-m zonal wind shows a northward shift (Fig. 6a), which is associated with the poleward shift of the jet (Manzini et al. 2018), and is considered as a robust response across the CMIP5 models for higher levels of greenhouse gas warming (Barnes and Polvani 2013). The effect of this shift can also be diagnosed in the northward shift of the zonal wind stress over the ocean, which extends the STG northward and causes anticyclonic circulation anomalies over the intergyre region (Fig. 6b). Further, the wind-driven Sverdrup transport shows a similar signature as the changes in the gyres (Figs. 6c and 3b). It indicates an anomalously positive Sverdrup transport at the intergyre region, where we also find the positive anomalies in gyre strength, confirming the major role of the wind forcing in this phase. This suggests that, if Earth continues to warm above 2 K, we might see a northward shift of the position of the STG due to the northward shift of the mean zonal wind.

Due to the northward shift of the STG, an anomalous anticyclonic circulation forms over the intergyre and over the southern part of the SPG (Fig. 3b). This anomalous circulation would recirculate the NAC, and hence the weakening NAC related salinity/density reduction seems to appear at the intergyre region (Figs. S2a,b). This implies that the salinity and associated density in the eastern side of the SPG does not reduce further like in the first phase of global warming, which results in no further intensification of the eastern to central SPG and leads to a stable state by keeping a steady density difference from the center of the SPG (Figs. 3b,c and 4a).

c. *Eastern subpolar gyre evolution and the warming hole*

The longitudinal cross section of the anomalous SST over the warming hole region (45°–55° N) shows a similar temporal

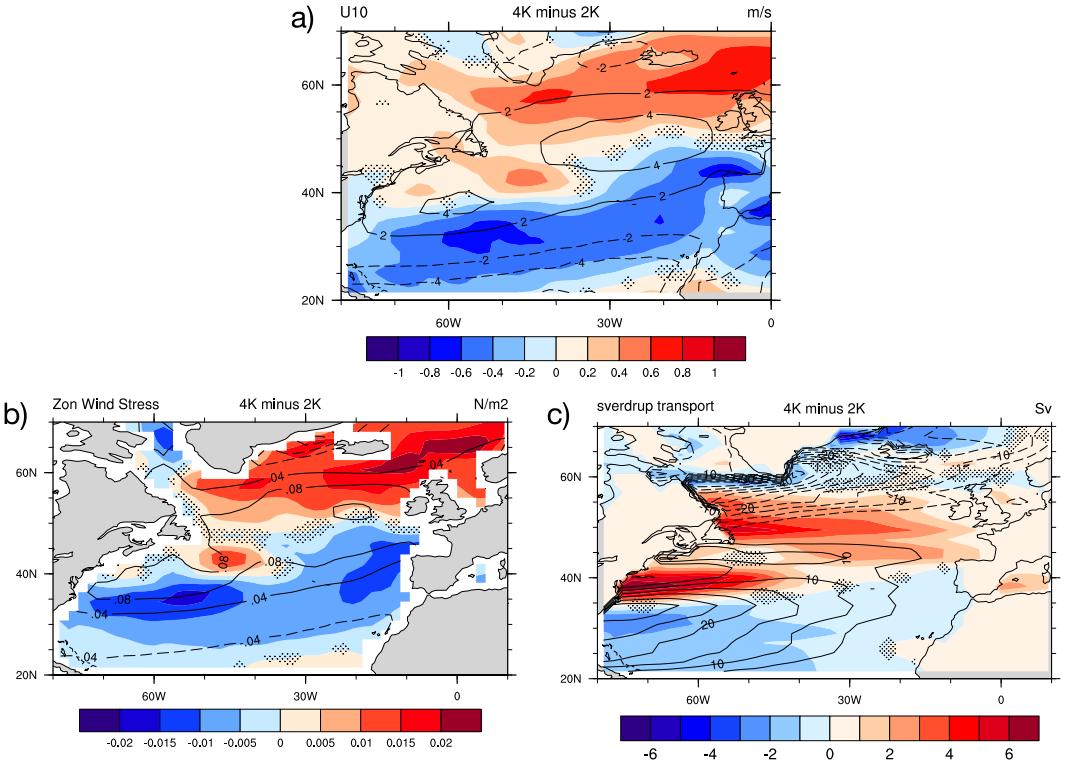

FIG. 6. (a) The difference of the ensemble mean annual zonal wind at 10 m (colors; m s^{-1}) between 4-K GMST warming and 2-K GMST warming levels in the MPI-GE 1% CO_2 increase per year experiment. Contours in (a) depict the ensemble mean annual 10-m zonal wind or the climatology 2-K GMST warming state. (b),(c) As in (a), but for the zonal wind stress on water (N m^{-2}) and for wind-driven Sverdrup transport (Sv), respectively. Negative values in (c) denote anomalous cyclonic circulation, and positive values denote anomalous anticyclonic circulation. The unstippled regions are statistically significant at $p < 0.05$.

evolution as for the eastern SPG (Figs. 3c,d). The WH intensifies as long as the eastern SPG intensifies in the model, which is until 2-K global warming. After which, the eastern SPG does not intensify further and the WH starts to cease, although the AMOC continues to weaken throughout both phases (red curve in Fig. 9). This indicates a direct link of the WH to eastern SPG evolution and a disconnect of the AMOC with the WH as well as with eastern SPG on a higher level of global warming under prominent changes in atmospheric circulations (Fig. 6).

d. *Association of eastern SPG changes to ocean meridional heat transport and warming hole*

In the 1% CO_2 experiment, the North Atlantic Ocean basinwide total meridional heat transport (MHT) shows significant reduction over time in the lower latitudes up until 40°, associated with the weakening AMOC related MHT (Figs. 7a,b). At higher latitudes (north of 50°N), an increasing total MHT is associated with both the AMOC and gyre related MHT (Fig. 7c), which is also a known feature in the twentieth century (Jungclaus et al. 2014; Oldenburg et al. 2018). Up until 2 K of global warming, the combination of a consistently weakening lower latitude and strengthening higher latitude total MHT create an increasing anomalous heat transport divergence (AHTD) at around 45°–50°N, which is shown to be one of the major drivers of the growing North Atlantic warming hole (WH) (Keil et al. 2020) (Fig. 4e). Interestingly, the evolution of the gyre related MHT at the subpolar region plays a crucial role in the development of this total AHTD (Fig. 7c) and in the nonlinear evolution of the WH (Fig. 3d). The initially increasing gyre MHT at the intergyre region (40°–50°N) leads to the increase of AHTD and the strengthening of the WH with increasing GMST warming of 2 K (Fig. 3d).

With further warming above 2 K, the gyre MHT decreases, effectively disrupting the growing AHTD at around 50°N, and hence diminishing the WH (Fig. 3d). The temporal evolution of the BSF averaged over the latitudes of the intergyre region shows a similar evolution in the associated gyre circulation at the eastern side of the ocean basin around 25°W (Fig. S3), where we also find the center of the warming hole in MPI-GE (Fig. 4e). Hence, SPG strengthening appears to be essential for the WH intensification. In addition, a strengthened SPG increases the mean heat transport toward the pole (Fig. 7a), which can enhance the Arctic sea ice melting (Fig. S4a).

5. Discussion

The chain of events which associates with the two distinct phases of changes in the eastern SPG under global warming are shown through a schematic in Fig. 8. In the first phase, the

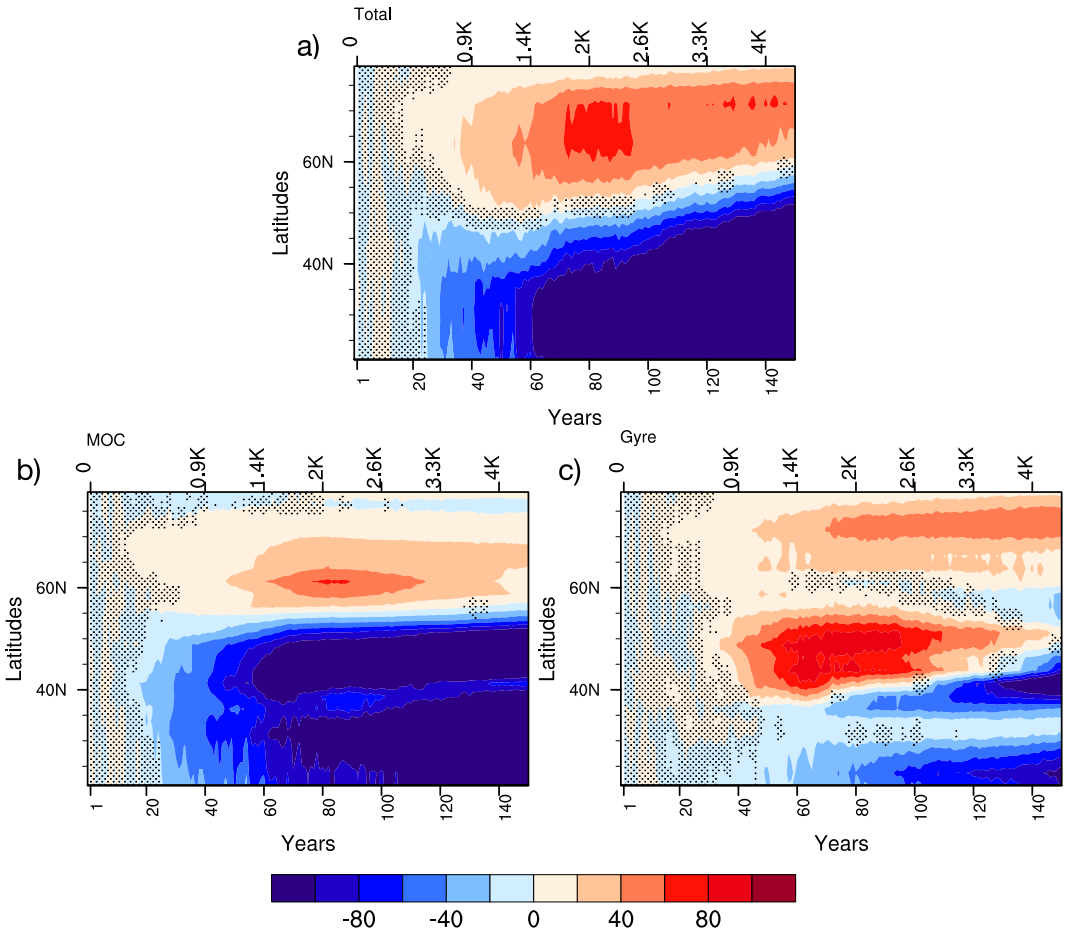

FIG. 7. In the MPI-GE 1% CO_2 increase per year experiment for 150 years, the difference of the ensemble mean annual basinwide meridional heat transport (MHT; TW, TW= 10^{12} W) for each year from the ensemble mean annual MHT of the first year at each latitude over the North Atlantic Ocean (0°–80°N) for the (a) total and its (b) MOC and (c) gyre components. The upper x axis shows the GMST warming level to a corresponding year. The differences that are significant at $p < 0.05$ are unstippled.

weakening of the AMOC (Fig. S4c) likely to have played a role to strengthen the eastern SPG through weakening the NAC, which freshens the eastern side of the SPG and creates larger east-to-center density difference. This strengthening eastern SPG led to an intensification of the WH and an increase of high latitude northward heat transport.

The second phase of global warming is when the strengthening of the eastern SPG and intensification of the WH cease in spite of a continuous decline of the AMOC (Fig. S4d). This cessation is associated with the northward shift of the mean zonal wind over the intergyre region which extends the STG northward and prohibits further enhancement of the east-to-center density difference in SPG. Hence, it is due to the shift of the main drivers from ocean to atmosphere which leads to the two distinct phases of eastern SPG changes under global warming in MPI-GE.

The AMOC weakening is found to be closely associated with the increased freshwater transport through the Denmark Strait (Fig. 9). Previous studies suggest that such increase in the freshwater transport could be related to the Arctic sea ice melting (Sévellec et al. 2017). However, increase in surface freshwater and heat fluxes are also suggested to weaken the AMOC (Gregory et al. 2005). Further research is required to determine the reason behind the increase in the Denmark Strait freshwater transport under global warming in the MPI-GE.

Regarding the changes in the North Atlantic centers of deep convection, the ocean mixed layer depth (MLD) indicates an important role of both Greenland–Iceland–Norwegian (GIN) Seas and Labrador Sea deep convection centers for the AMOC weakening (Fig. 10). Evidently in both phases of the global warming, the MLD weakens in these two centers of the deep convection (Figs. 10a,b). In the first phase, the magnitude of the weakening is stronger compared to the second. Moreover, in the first phase, the reduction in the MLD is larger over the GIN Seas compared to the Labrador Sea (Fig. 10a). The MLD weakening could be seen spread over the north-eastern side of the SPG. This finding suggests that AMOC weakening in MPI-

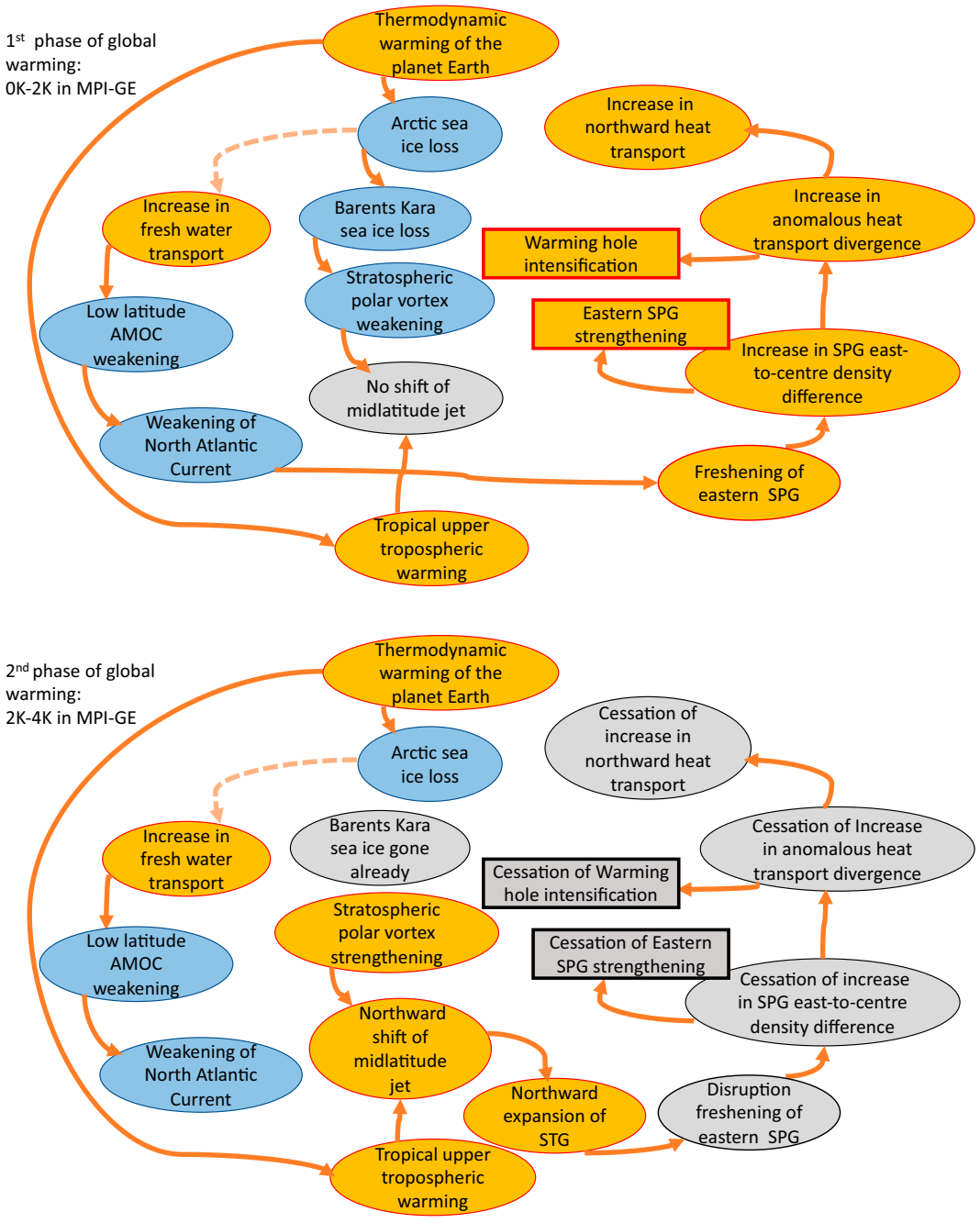

FIG. 8. Schematic diagrams showing the connections in between the processes described in the results over the North Atlantic SPG region for the (a) first phase and (b) second phase of the global warming in the MPI-GE. The orange colors denote the positive change/increase, blue denotes negative change/decrease, and gray denotes no change in a parameter. The faded dashed line indicates a possible but unproven link. The red and black boxes highlight the central parameter of this study.

GE under global warming can be related to the changes in the strength of the deep convection in both eastern and western side of subpolar North Atlantic.

In the second phase of the global warming, the northward shift of the mean zonal wind plays a key role in changing the North Atlantic gyre circulations. Using the same experimental data, Manzini et al. (2018) has shown that a change in the strength of the Stratospheric polar vortex (SPV) from the first to the second phase of global warming plays an important role for the northward shift of the mean zonal wind. The

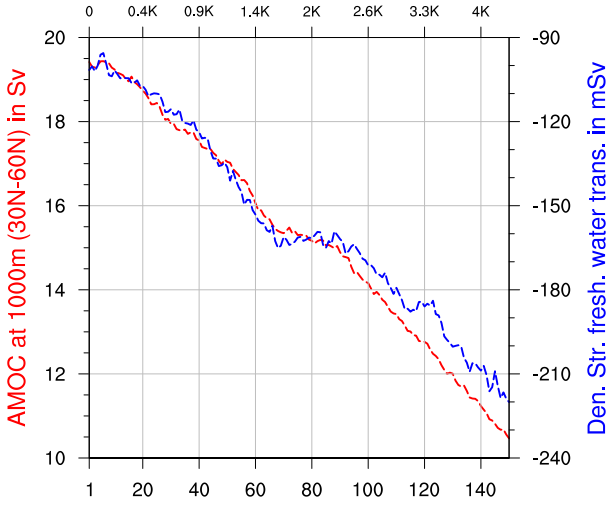

FIG. 9. In the MPI-GE 1% CO_2 experiment, the time series of the maximum AMOC strength (in red) at 1000-m depth (Sv), averaged over the latitude 30°–60°N and the integrated freshwater transport through the Denmark Strait (blue; mSv; minus sign indicates southward transport). The bottom x axis shows the simulation years, and the top x axis shows the corresponding GMST warming level.

change in the strength of the SPV is also linked with the change in the state of the Arctic sea ice, especially over the Barents and Kara Seas (Manzini et al. 2018; Kretschmer et al. 2020). During the first phase of global warming, the SPV would weaken due to the major sea ice loss over BKS (Fig. S4a). During the second phase, most of the BKS sea ice is gone (Fig. S4b) and SPV would strengthen, which in combination with the tropical upper troposphere warming leads to the poleward movement of the mean zonal winds. However, previous studies also suggest other ways by which a northward shift of zonal mean wind could happen. For example, the Hadley cell expansion (Mbengue and Schneider 2013, 2017) or the changes in the cloud radiative effect from global warming (Voigt and Shaw 2015) could also lead to a northward shift of the mean zonal wind over the midlatitudes. The possible role of these processes in MPI-GE are yet to be explored.

Our results show a crucial role of both the AMOC and the gyre related heat transports behind the formation and the intensification of the North Atlantic WH through creating a heat transport divergence at the sub polar latitudes (Fig. 7). The gyre related heat transport is found to be a crucial indicator. Because we find the decline in the WH intensification with an associated decrease in the gyre heat transport. A close link between the SPG changes and the WH is also found in the large ensemble simulation of the Community Earth System Model, though the suggested mechanism differs with a more crucial role of the western SPG that the east (Gervais et al. 2018). This indicates the potential of different oceanic mechanisms leading to a WH over subpolar North Atlantic Ocean. Apart from the oceanic processes, the previous studies also find possibilities of the WH formation driven by atmospheric processes (Keil et al. 2020; Menary and Wood 2018). For example, ocean surface heat loss due to local atmospheric forcing (Li et al. 2022) or changes in the local cloud feedback (Keil et al. 2020) are also found to lead to a WH.

We acknowledge that the eastern SPG response to anthropogenic forcing in MPI-GE could be different in other models as there are known uncertainties in future SPG evolution among models (Reintges et al. 2017). However, the similarity of our model subsurface signatures with the observations in the strengthening phase of eastern SPG makes the MPI-GE simulated forced response a reliable contender of a possible future SPG state under anthropogenic forcing. Although we should note that the model eastern SPG response is found southeast ward compared to the observations. This is a result of a southward and eastward extended climatological SPG in the MPI-GE due to a zonal nature of the NAC (Fig. 2). This zonal nature of the model NAC could have implications for our findings on the second phase of global warming. The potential influence of the northward shift of the zonal mean wind on the observed North Atlantic STG extension and on the WH could be of different magnitude compared to the MPI-GE.

Finally, this study demonstrates how the shift of influence from the ocean to the atmosphere could lead to a regime shift in the North Atlantic Ocean SPG circulation evolution and its associated SST under monotonically increasing global warming. In the first phase, the oceanic processes dominate with a

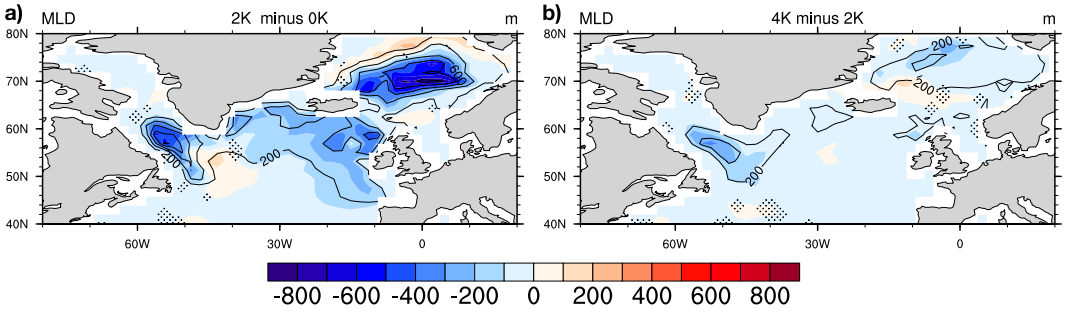

FIG. 10. The difference of the ensemble mean mixed layer depth (MLD; colors; m) (a) between 2-K global mean surface air temperature (GMST) warming and 0-K GMST warming levels and (b) between 4-K GMST warming and 2-K GMST warming levels in MPI-GE 1% CO_2 experiment. Contours are the ensemble mean annual MLD or the climatology for the 0- and (b) 2-K GMST warming state in (a) and (b), respectively. Contours are drawn starting from 200 m with an increasing 200-m interval. The unstippled regions are statistically significant at $p < 0.05$.

weakening AMOC being associated with the strengthening eastern SPG and intensifying the North Atlantic WH. However, in the second phase, the SPG circulation is determined by the atmospheric processes through the shift in the mean zonal wind over the midlatitudes disrupting the eastern SPG intensification and ceasing the WH intensification. Understanding the processes behind the transition from the ocean to the atmosphere driven changes of the subpolar North Atlantic is crucial due to its consequences for the downstream European climate variability and extremes (Haarsma et al. 2015; Ghosh et al. 2017; Mecking et al. 2019; Krüger et al. 2020). Moreover, the changes in the SPG are directly linked to regional sea level change and can have an effect on the local biogeochemical and ecological aspects. Hence looking at the overarching influences of the North Atlantic SPG, this study recommends more focus especially on the SPG evolution and its dynamics, for understanding the development of the Northern Hemispheric continental climate and its variability under anthropogenic warming.

Acknowledgments. We are thankful for the comments on the draft from Chao Li, Dirk Olonscheck, and Jochem Marotzke. The research leading to these results has received funding from EU H2020 Blue-Action (Grant 727852) (RG, DM, EM, KL), EU H2020 AtlantOS (Grant 633211) (RG, JJ), EU H2020 PRIMAVERA (Grant 641727) (JJ, DP, KL), and the German Federal Ministry of Education and Research (BMBF) through the JPI Climate/JPI Oceans NextG-Climate Science-ROADMAP (FKZ: 01LP2002A) (DM, EM, KL, JB) and RACE-II (FKZ03FO729D) (DM, JJ) projects. Computational resources are provided by the Deutsches Klimarechenzentrum (DKRZ), BMBF, and Swiss National Supercomputing Center (CSCS). We are thankful to JAMSTEC and Copernicus marine environment monitoring service (CMEMS) for providing the Argo float and the Satellite altimeter observations, respectively.

Data availability statement. The MPI-GE data from all the experiments are publicly available at ESGF (https://esgf-data.dkrz.de/projects/esgf-dkrz/). DUACS DT2014 multi-satellite altimeter data for sea surface height can be found at http://marine.copernicus.eu/services-portfolio/access-to-products/ provided by Copernicus marine environment monitoring service (CMEMS). The gridded salinity observations from Argo float data can be retrieved on request from http://www.jamstec.go.jp/ARGO/argoweb/argo/.

REFERENCES

Barnes, E. A., and L. Polvani, 2013: Response of the midlatitude jets, and of their variability, to increased greenhouse gases in the CMIP5 models. *J. Climate*, **26**, 7117–7135, https://doi.org/10.1175/JCLI-D-12-00536.1.

Beadling, R. L., J. L. Russell, R. J. Stouffer, and P. J. Goodman, 2018: Evaluation of subtropical North Atlantic Ocean circulation in CMIP5 models against the observational array at 26.5°N and its changes under continued warming. *J. Climate*, **31**, 9697–9718, https://doi.org/10.1175/JCLI-D-17-0845.1.

Böning, C. W., M. Scheinert, J. Dengg, A. Biastoch, and A. Funk, 2006: Decadal variability of subpolar gyre transport and its reverberation in the North Atlantic overturning. *Geophys. Res. Lett.*, **33**, L21S01, https://doi.org/10.1029/2006GL026906.

Born, A., and T. F. Stocker, 2014: Two stable equilibria of Atlantic subpolar gyre. *J. Phys. Oceanogr.*, **44**, 246–264, https://doi.org/10.1175/JPO-D-13-073.1.

Bryan, K., 1982: Poleward heat transport by the ocean: Observations and models. *Annu. Rev. Earth Planet. Sci.*, **10**, 15–38, https://doi.org/10.1146/annurev.ea.10.050182.000311.

Bryden, H. L., W. E. Johns, B. A. King, G. McCarthy, E. L. McDonagh, B. I. Moat, and D. A. Smeed, 2020: Reduction in ocean heat transport at 26°N since 2008 cools the eastern subpolar gyre of the North Atlantic Ocean. *J. Climate*, **33**, 1677–1689, https://doi.org/10.1175/JCLI-D-19-0323.1.

Carpenter, E. J., and K. L. Smith, 1972: Plastics on the Sargasso Sea surface. *Science*, **175**, 1240–1241, https://doi.org/10.1126/science.175.4027.1240.

Chafik, L., J. E. Ø. Nilsen, S. Dangendorf, G. Reverdin, and T. Frederikse, 2019: North Atlantic Ocean circulation and decadal sea level change during the altimetry era. *Sci. Rep.*, **9**, 1041, https://doi.org/10.1038/s41598-018-37603-6.

Cheng, W., J. C. H. Chiang, and D. Zhang, 2013: Atlantic meridional overturning circulation (AMOC) in CMIP5 models: RCP and historical simulations. *J. Climate*, **26**, 7187–7197, https://doi.org/10.1175/JCLI-D-12-00496.1.

Colton, J. B., B. R. Burns, and F. D. Knapp, 1974: Plastic particles in surface waters of the northwestern Atlantic. *Science*, **185**, 491–497, https://doi.org/10.1126/science.185.4150.491.

Daniault, N., H. Mercier, and P. Lherminier, 2011: The 1992–2009 transport variability of the East Greenland–Irminger Current at 60°N. *Geophys. Res. Lett.*, **38**, L07601, https://doi.org/10.1029/2011GL046863.

Drijfhout, S., G. J. van Oldenborgh, and A. Cimatoribus, 2012: Is a decline of AMOC causing the warming hole above the North Atlantic in observed and modeled warming patterns? *J. Climate*, **25**, 8373–8379, https://doi.org/10.1175/JCLI-D-12-00490.1.

Foukal, N. P., and M. S. Lozier, 2017: Assessing variability in the size and strength of the North Atlantic subpolar gyre. *J. Geophys. Res. Oceans*, **122**, 6295–6308, https://doi.org/10.1002/2017JC012798.

Gervais, M., J. Shaman, and Y. Kushnir, 2018: Mechanisms governing the development of the North Atlantic warming hole in the CESM-LE future climate simulations. *J. Climate*, **31**, 5927–5946, https://doi.org/10.1175/JCLI-D-17-0635.1.

Ghosh, R., W. A. Müller, J. Baehr, and J. Bader, 2017: Impact of observed North Atlantic multidecadal variations to European summer climate: A linear baroclinic response to surface heating. *Climate Dyn.*, **48**, 3547–3563, https://doi.org/10.1007/s00382-016-3283-4.

Giorgetta, M. A., and Coauthors, 2013: Climate and carbon cycle changes from 1850 to 2100 in MPI-ESM simulations for the Coupled Model Intercomparison Project Phase 5. *J. Adv. Model. Earth Syst.*, **5**, 572–597, https://doi.org/10.1002/jame.20038.

Gregory, J. M., and Coauthors, 2005: A model intercomparison of changes in the Atlantic thermohaline circulation in response to increasing atmospheric CO_2 concentration. *Geophys. Res. Lett.*, **32**, L12703, https://doi.org/10.1029/2005GL023209.

Griffies, S. M., and Coauthors, 2016: OMIP contribution to CMIP6: Experimental and diagnostic protocol for the physical component of the ocean model intercomparison project.

Geosci. Model Dev., **9**, 3231–3296, https://doi.org/10.5194/gmd-9-3231-2016.

Haarsma, R. J., F. M. Selten, and S. S. Drijfhout, 2015: Decelerating Atlantic meridional overturning circulation main cause of future west European summer atmospheric circulation changes. *Environ. Res. Lett.*, **10**, 094007, https://doi.org/10.1088/1748-9326/10/9/094007.

Häkkinen, S., and P. B. Rhines, 2004: Decline of subpolar North Atlantic circulation during the 1990s. *Science*, **304**, 555–559, https://doi.org/10.1126/science.1094917.

Hand, R., J. Bader, D. Matei, R. Ghosh, and J. H. Jungclaus, 2020: Changes of decadal SST variations in the subpolar North Atlantic under strong CO_2 forcing as an indicator for the ocean circulations contribution to Atlantic multidecadal variability. *J. Climate*, **33**, 3213–3228, https://doi.org/10.1175/JCLI-D-18-0739.1.

Hátún, H., and L. Chafik, 2018: On the recent ambiguity of the North Atlantic subpolar gyre index. *J. Geophys. Res. Oceans*, **123**, 5072–5076, https://doi.org/10.1029/2018JC014101.

——, A. B. Sandø, H. Drange, B. Hansen, and H. Valdimarsson, 2005: Influence of the Atlantic subpolar gyre on the thermohaline circulation. *Science*, **309**, 1841–1844, https://doi.org/10.1126/science.1114777.

——, and Coauthors, 2009: Large bio-geographical shifts in the north-eastern Atlantic Ocean: From the subpolar gyre, via plankton, to blue whiting and pilot whales. *Prog. Oceanogr.*, **80**, 149–162, https://doi.org/10.1016/j.pocean.2009.03.001.

——, K. Lohmann, D. Matei, J. H. Jungclaus, S. Pacariz, M. Bersch, and A. Gislason, 2016: An inflated subpolar gyre blows life toward the northeastern Atlantic. *Prog. Oceanogr.*, **147**, 49–66, https://doi.org/10.1016/j.pocean.2016.07.009.

——, and Coauthors, 2017: The subpolar gyre regulates silicate concentrations in the North Atlantic. *Sci. Rep.*, **7**, 14576, https://doi.org/10.1038/s41598-017-14837-4.

Hermanson, L., R. Eade, N. H. Robinson, N. J. Dunstone, M. B. Andrews, J. R. Knight, A. A. Scaife, and D. M. Smith, 2014: Forecast cooling of the Atlantic subpolar gyre and associated impacts. *Geophys. Res. Lett.*, **41**, 5167–5174, https://doi.org/10.1002/2014GL060420.

Hosoda, S., T. Ohira, and T. Nakamura, 2008: A monthly mean dataset of global oceanic temperature and salinity derived from Argo float observations. *JAMSTEC Rep. Res. Dev.*, **8**, 47–59, https://doi.org/10.5918/jamstecr.8.47.

Ilyina, T., K. D. Six, J. Segschneider, E. Maier-Reimer, H. Li, and I. Núñez-Riboni, 2013: Global ocean biogeochemistry model HAMOCC: Model architecture and performance as component of the MPI-earth system model in different CMIP5 experimental realizations. *J. Adv. Model. Earth Syst.*, **5**, 287–315, https://doi.org/10.1029/2012MS000178.

Jalali, B., M.-A. Sicre, J. Azuara, V. Pellichero, and N. Combourieu-Nebout, 2019: Influence of the North Atlantic subpolar gyre circulation on the 4.2 ka BP event. *Climate Past*, **15**, 701–711, https://doi.org/10.5194/cp-15-701-2019.

Jenkins, W. J., 1982: Oxygen utilization rates in North Atlantic subtropical gyre and primary production in oligotrophic systems. *Nature*, **300**, 246–248, https://doi.org/10.1038/300246a0.

Jungclaus, J. H., and Coauthors, 2013: Characteristics of the ocean simulations in the Max Planck Institute Ocean Model (MPIOM) the ocean component of the MPI—Earth system model. *J. Adv. Model. Earth Syst.*, **5**, 422–446, https://doi.org/10.1002/jame.20023.

——, A. Macrander, and R. H. Käse, 2008: Modelling the overflows across the Greenland–Scotland Ridge. *Arctic–Subarctic Ocean Fluxes*, R. R. Dickson, J. Meincke, and P. Rhines, Eds., Springer, 527–549.

——, K. Lohmann, and D. Zanchettin, 2014: Enhanced 20th-century heat transfer to the Arctic simulated in the context of climate variations over the last millennium. *Climate Past*, **10**, 2201–2213, https://doi.org/10.5194/cp-10-2201-2014.

Keil, P., T. Mauritsen, J. Jungclaus, C. Hedemann, D. Olonscheck, and R. Ghosh, 2020: Multiple drivers of the North Atlantic warming hole. *Nat. Climate Change*, **10**, 667–671, https://doi.org/10.1038/s41558-020-0819-8.

Kretschmer, M., G. Zappa, and T. G. Shepherd, 2020: The role of Barents–Kara sea ice loss in projected polar vortex changes. *Wea. Climate Dyn.*, **1**, 715–730, https://doi.org/10.5194/wcd-1-715-2020.

Krüger, J., R. Pilch Kedzierski, K. Bumke, and K. Matthes, 2020: Impact of North Atlantic SST and jet stream anomalies on European heat waves. *Wea. Climate Dyn. Discuss.*, https://doi.org/10.5194/wcd-2020-32, in press.

Law, K. L., S. Morét-Ferguson, N. A. Maximenko, G. Proskurowski, E. E. Peacock, J. Hafner, and C. M. Reddy, 2010: Plastic accumulation in the North Atlantic subtropical gyre. *Science*, **329**, 1185–1188, https://doi.org/10.1126/science.1192321.

Levermann, A., and A. Born, 2007: Bistability of the Atlantic subpolar gyre in a coarse-resolution climate model. *Geophys. Res. Lett.*, **34**, L24605, https://doi.org/10.1029/2007GL031732.

Li, H., and T. Ilyina, 2018: Current and future decadal trends in the oceanic carbon uptake are dominated by internal variability. *Geophys. Res. Lett.*, **45**, 916–925, https://doi.org/10.1002/2017GL075370.

Li, L., M. S. Lozier, and F. Li, 2022: Century-long cooling trend in subpolar North Atlantic forced by atmosphere: An alternative explanation. *Climate Dyn.*, **58**, 2249–2267, https://doi.org/10.1007/s00382-021-06003-4.

Lohmann, K., H. Drange, and M. Bentsen, 2009a: Response of the North Atlantic subpolar gyre to persistent North Atlantic oscillation like forcing. *Climate Dyn.*, **32**, 273–285, https://doi.org/10.1007/s00382-008-0467-6.

——, ——, and ——, 2009b: A possible mechanism for the strong weakening of the North Atlantic subpolar gyre in the mid-1990s. *Geophys. Res. Lett.*, **36**, L15602, https://doi.org/10.1029/2009GL039166.

Maher, N., and Coauthors, 2019: The Max Planck Institute grand ensemble: Enabling the exploration of climate system variability. *J. Adv. Model. Earth Syst.*, **11**, 2050–2069, https://doi.org/10.1029/2019MS001639.

Manabe, S., and R. J. Stouffer, 1993: Century-scale effects of increased atmospheric CO_2 on the ocean-atmosphere system. *Nature*, **364**, 215–218, https://doi.org/10.1038/364215a0.

Manzini, E., A. Y. Karpechko, and L. Kornblueh, 2018: Nonlinear response of the stratosphere and the North Atlantic-European climate to global warming. *Geophys. Res. Lett.*, **45**, 4255–4263, https://doi.org/10.1029/2018GL077826.

Marsland, S. J., H. Haak, J. H. Jungclaus, M. Latif, and F. Röeske, 2003: The Max-Planck-Institute global ocean/sea ice model with orthogonal curvilinear coordinates. *Ocean Model.*, **5**, 91–127, https://doi.org/10.1016/S1463-5003(02)00015-X.

Mbengue, C., and T. Schneider, 2013: Storm track shifts under climate change: What can be learned from large-scale dry dynamics. *J. Climate*, **26**, 9923–9930, https://doi.org/10.1175/JCLI-D-13-00404.1.

——, and ——, 2017: Storm-track shifts under climate change: Toward a mechanistic understanding using baroclinic mean

available potential energy. *J. Atmos. Sci.*, **74**, 93–110, https://doi.org/10.1175/JAS-D-15-0267.1.

Mecking, J. V., S. S. Drijfhout, J. J.-M. Hirschi, and A. T. Blaker, 2019: Ocean and atmosphere influence on the 2015 European heatwave. *Environ. Res. Lett.*, **14**, 114035, https://doi.org/10.1088/1748-9326/ab4d33.

Menary, M. B., and R. A. Wood, 2018: An anatomy of the projected North Atlantic warming hole in CMIP5 models. *Climate Dyn.*, **50**, 3063–3080, https://doi.org/10.1007/s00382-017-3793-8.

Moffa-Sánchez, P., and I. R. Hall, 2017: North Atlantic variability and its links to European climate over the last 3000 years. *Nat. Commun.*, **8**, 1726, https://doi.org/10.1038/s41467-017-01884-8.

Moreno-Chamarro, E., D. Zanchettin, K. Lohmann, and J. H. Jungclaus, 2017a: An abrupt weakening of the subpolar gyre as trigger of little ice age-type episodes. *Climate Dyn.*, **48**, 727–744, https://doi.org/10.1007/s00382-016-3106-7.

——, ——, ——, J. Luterbacher, and J. H. Jungclaus, 2017b: Winter amplification of the European little ice age cooling by the subpolar gyre. *Sci. Rep.*, **7**, 9981, https://doi.org/10.1038/s41598-017-07969-0.

Oldenburg, D., K. C. Armour, L. A. Thompson, and C. M. Bitz, 2018: Distinct mechanisms of ocean heat transport into the Arctic under internal variability and climate change. *Geophys. Res. Lett.*, **45**, 7692–7700, https://doi.org/10.1029/2018GL078719.

Palter, J. B., M. S. Lozier, and R. T. Barber, 2005: The effect of advection on the nutrient reservoir in the North Atlantic subtropical gyre. *Nature*, **437**, 687–692, https://doi.org/10.1038/nature03969.

Pujol, M.-I., Y. Faugère, G. Taburet, S. Dupuy, C. Pelloquin, M. Ablain, and N. Picot, 2016: DUACS DT2014: The new multi-mission altimeter data set reprocessed over 20 years. *Ocean Sci.*, **12**, 1067–1090, https://doi.org/10.5194/os-12-1067-2016.

Rahmstorf, S., J. E. Box, G. Feulner, M. E. Mann, A. Robinson, S. Rutherford, and E. J. Schaffernicht, 2015: Exceptional twentieth-century slowdown in Atlantic Ocean overturning circulation. *Nat. Climate Change*, **5**, 475–480, https://doi.org/10.1038/nclimate2554.

Reick, C. H., T. Raddatz, V. Brovkin, and V. Gayler, 2013: Representation of natural and anthropogenic land cover change in MPI-ESM. *J. Adv. Model. Earth Syst.*, **5**, 459–482, https://doi.org/10.1002/jame.20022.

Reintges, A., T. Martin, M. Latif, and N. S. Keenlyside, 2017: Uncertainty in twenty-first century projections of the Atlantic meridional overturning circulation in CMIP3 and CMIP5 models. *Climate Dyn.*, **49**, 1495–1511, https://doi.org/10.1007/s00382-016-3180-x.

Richter, K., J. E. Øie Nilsen, R. P. Raj, I. Bethke, J. A. Johannessen, A. B. A. Slangen, and B. Marzeion, 2017: Northern North Atlantic sea level in CMIP5 climate models: Evaluation of mean state, variability, and trends against altimetric observations. *J. Climate*, **30**, 9383–9398, https://doi.org/10.1175/JCLI-D-17-0310.1.

Robson, J., P. Ortega, and R. Sutton, 2016: A reversal of climatic trends in the North Atlantic since 2005. *Nat. Geosci. Lett.*, **9**, 513–518, https://doi.org/10.1038/ngeo272.

Schmittner, A., M. Latif, and B. Schneider, 2005: Model projections of the North Atlantic thermohaline circulation for the 21st century assessed by observations. *Geophys. Res. Lett.*, **32**, L23710, https://doi.org/10.1029/2005GL024368.

Sévellec, F., A. V. Fedorov, and W. Liu, 2017: Arctic sea-ice decline weakens the Atlantic meridional overturning circulation. *Nat. Climate Change*, **7**, 604–610, https://doi.org/10.1038/nclimate3353.

Smeed, D. A., and Coauthors, 2014: Observed decline of the Atlantic meridional overturning circulation 2004–2012. *Ocean Sci.*, **10**, 29–38, https://doi.org/10.5194/os-10-29-2014.

——, and Coauthors, 2018: The North Atlantic Ocean is in a state of reduced overturning. *Geophys. Res. Lett.*, **45**, 1527–1533, https://doi.org/10.1002/2017GL076350.

Stevens, B., and Coauthors, 2013: Atmospheric component of the MPI-M earth system model: ECHAM6. *J. Adv. Model. Earth Syst.*, **5**, 146–172, https://doi.org/10.1002/jame.20015.

Stocker, T. F., and A. Schmittner, 1997: Influence of CO_2 emission rates on the stability of the thermohaline circulation. *Nature*, **388**, 862–865, https://doi.org/10.1038/42224.

Voigt, A., and T. A. Shaw, 2015: Circulation response to warming shaped by radiative changes of clouds and water vapour. *Nat. Geosci.*, **8**, 102–106, https://doi.org/10.1038/ngeo2345.

Yeager, S., 2015: Topographic coupling of the Atlantic overturning and gyre circulations. *J. Phys. Oceanogr.*, **45**, 1258–1284, https://doi.org/10.1175/JPO-D-14-0100.1.

Zhang, R., 2008: Coherent surface-subsurface fingerprint of the Atlantic meridional overturning circulation. *Geophys. Res. Lett.*, **35**, L20705, https://doi.org/10.1029/2008GL035463.